An improved kinetics model to describe dynamic recrystallization behavior under inconstant deformation conditions

Ming-Song Chen[a] and Kuo-Kuo Li
School of Mechanical and Electrical Engineering, Central South University, Changsha 410083, China; and State Key Laboratory of High Performance Complex Manufacturing, Changsha 410083, China

Yong-Cheng Lin[b]
School of Mechanical and Electrical Engineering, Central South University, Changsha 410083, China; State Key Laboratory of High Performance Complex Manufacturing, Changsha 410083, China; and Light Alloy Research Institute of Central South University, Changsha 410083, China

Wu-Quan Yuan
School of Mechanical and Electrical Engineering, Central South University, Changsha 410083, China; and State Key Laboratory of High Performance Complex Manufacturing, Changsha 410083, China

(Received 11 July 2016; accepted 19 August 2016)

The classical dynamic recrystallization (DRX) kinetics models, such as Avrami equation, are often used to describe the DRX behaviors of alloys. However, it is found that the classical DRX kinetics models cannot be directly applied to evaluate DRX volume fractions under inconstant deformation conditions, such as at fluctuant deformation temperature and strain rate. It obviously limits their application in the practical industrial production. Therefore, an improved DRX kinetics model is proposed based on the hypothesis that the derivatives of DRX volume fraction with respect to strain only depends on the current deformation temperature, strain rate, and DRX volume fraction. To verify the improved DRX kinetics model, the hot compressive tests in which the strain rate is inconstant are carried out on a solution-treated Ni-based superalloy. Experimental results indicate that the improved DRX kinetics model can well predict the DRX behavior under inconstant deformation conditions.

I. INTRODUCTION

Dynamic recrystallization (DRX) is one of most important microstructural evolution mechanisms for most of metals and alloys during hot deformation, such as forging. During DRX, the initial coarse-grains are gradually replaced by fine DRX grains. The final microstructures of forgings greatly depend on the DRX volume fraction and grain size.[1,2] Incomplete DRX, where the DRX volume fraction is less than 95%, will result in serious mixed structures with fine and coarse grains. This is not permitted or expected since the mixed structure will seriously deteriorate the mechanical properties for most materials. Therefore, it is very significant to precisely predict and control the DRX volume fraction of forgings after hot deformation.

The DRX kinetics model is essential to predict and control the DRX volume fraction of forgings. In recent decades, some efforts have been made to investigate the DRX behaviors and kinetics models of various metals and alloys, such as Nb-steels,[3,4] Aermet100 steel,[5] 38MnVS6 Steel,[6] 42CrMo steel,[7] a low carbon vanadium-nitride microalloyed steel,[8] SCM435 steel,[9] 300M steel,[10] 17-4 PH stainless steel,[11] X70 pipeline steel,[12] titanium-modified austenitic stainless steel,[13] 410 martensitic stainless steel,[14] superaustenitic stainless steel,[15] 304 stainless steel,[16–18] martensitic stainless steel,[19] high purity and ultra-high purity austenitic stainless steels,[20] Cu-0.4 Mg alloy,[21] magnesium alloys,[22] Mg–Y–Nd–Zr alloy,[23] Mg–Li–Al–Nd duplex alloy,[24] Mg–Gd–Y–Zr alloy,[25] Mg–2.0Zn–0.3Zr alloy,[26] TiAl alloy,[27] Ti55511 titanium alloy,[28] FGH4096 superalloy,[29] and typical Ni-based superalloys.[30–34] In these works, hot compressive or tensile tests with constant deformation temperature and strain rate were usually used to investigate the effects of thermomechanical parameters (temperature, strain rate, and strain), chemical compositions,[3] initial grain size,[7,18,20] and precipitates[4,22,33,35–37] on DRX behaviors. The DRX volume fractions of materials were often evaluated by analyzing true stress-true strain curves.[28,38,39] It was found that the dependence of DRX volume fraction on strain under constant deformation temperature and strain rate can be described by the Avrami equation.[40] Therefore, the Avrami equation is often applied to describe the DRX kinetics behavior. ε_c (the critical strain for the onset of DRX),

Contributing Editor: Mathias Göken
Address all correspondence to these authors.
[a]e-mail: chenms18@csu.edu.cn
[b]e-mail: yclin@csu.edu.cn
DOI: 10.1557/jmr.2016.325

 © Materials Research Society 2016

https://doi.org/10.1557/jmr.2016.325 Published online by Cambridge University Press

$\varepsilon_{0.5}$ (the strain for 50% DRX), ε_p (the strain for peak stress), and ε^* (the strain for maximum softening rate) are the characteristic parameters of kinetics models. The characteristic parameters are often expressed as the functions of deformation temperature and strain rate[34] or Zener–Hollomon parameter.[8,12,19,21,24,31] For some researches,[7,10,18,20] the effect of initial grain size on DRX behaviors was considered. Thus, the characteristic parameters are also expressed as the functions of initial grain size, deformation temperature and strain rate. Besides the Avrami equation, Liu et al.[41] proposed a new DRX kinetics model which can represent the 'slow–rapid–slow' property of DRX development. It is well known that the classical DRX kinetics models can be expediently used to predict the DRX volume fractions under constant deformation temperature and strain rate, because the characteristic parameters, such as ε_c, ε_p, $\varepsilon_{0.5}$, and ε^*, remain constant. However, the real deformation temperature and strain rate of metals and alloys during hot deformation are often time-varying.[42] So, it is very important to evaluate the DRX volume fractions under inconstant deformation temperature and strain rate. But, there will be a question when the classical DRX kinetics models are applied to evaluate the DRX volume fractions under inconstant deformation temperature and strain rate. i.e., the characteristic parameters (ε_c, ε_p, $\varepsilon_{0.5}$, and ε^*) should be calculated by which deformation temperature and strain rate? Obviously, the classic DRX kinetics models cannot be directly applied in inconstant deformation temperature and strain rate conditions. Therefore, the classic DRX kinetics models need to be improved.

In this study, an improved DRX kinetics model, which can well describe the DRX kinetics under inconstant deformation temperature and strain rate conditions, is proposed. The proposition of improved model is based on the hypothesis that the derivatives of DRX volume fraction with respect to strain only depends on the current deformation temperature, strain rate, and DRX volume fraction. To verify the improved model, the hot compressive tests under the variant strain rate were carried out on a typical solution-treated Ni-based superalloy.

II. THE PROPOSITION OF AN IMPROVED DRX KINETICS MODEL

A. Classical DRX kinetics models

The general form of classical DRX kinetics models can be expressed as:

$$X_{drx} = 1 - \exp\left[-k\left(\frac{\varepsilon - \varepsilon_c}{\varepsilon'}\right)^n\right] \quad , \qquad (1)$$

where ε is the strain, X_{drx} is the DRX volume fraction at the strain of ε, ε_c is the critical strain for the onset of DRX, ε' can be a particular strain such as ε^* (the strain for maximum softening rate),[26,43–45] ε_p (the strain for peak stress),[8,10,46] ε_c (the critical strain for the onset of DRX),[5,21] and $(\varepsilon_{0.5} - \varepsilon_c)$,[7,31,34] n is the material constant (Avrami exponent) related to the DRX nucleation mechanism, and k is a constant related to ε' or materials.

When ε' is $(\varepsilon_{0.5} - \varepsilon_c)$, the value of k is 0.693 (or $-\ln 0.5$). i.e., Eq. (1) can be changed as:

$$X_{drx} = 1 - \exp\left[-0.693\left(\frac{\varepsilon - \varepsilon_c}{\varepsilon_{0.5} - \varepsilon_c}\right)^n\right] \quad . \qquad (2)$$

For some metals and alloys, $(\varepsilon_{0.5} - \varepsilon_c)$ is usually replaced by $\varepsilon_{0.5}$ since $\varepsilon_{0.5}$ is often much larger than ε_c. i.e., the following equation is also widely used to describe the DRX kinetics.[47–49]

$$X_{drx} = 1 - \exp\left[-0.693\left(\frac{\varepsilon - \varepsilon_c}{\varepsilon_{0.5}}\right)^n\right] \quad . \qquad (3)$$

Usually, ε_c and $\varepsilon_{0.5}$ can be expressed as the functions of deformation temperature (T, unit: K) and strain rate ($\dot{\varepsilon}$, unit: s^{-1}).[34]

$$\begin{cases} \varepsilon_c = a_1 \dot{\varepsilon}^{m_1} \exp(Q_1/T) \\ \varepsilon_{0.5} = a_2 \dot{\varepsilon}^{m_2} \exp(Q_2/T) \end{cases} \qquad (4)$$

in which a_1, a_2, m_1, m_2, Q_1, and Q_2 are material constants. ε_c and $\varepsilon_{0.5}$ can also be expressed as the functions of Zener–Hollomon parameter (Z).

$$\begin{cases} \varepsilon_c = a_1 Z^{m_1} \\ \varepsilon_{0.5} = a_2 Z^{m_2} \\ Z = \dot{\varepsilon} \exp[Q/(RT)] \end{cases} \qquad (5)$$

in which Q is the deformation activation energy (J/mol) and R is the universal gas constant [8.314 J/(mol K)].

When $\varepsilon' = \varepsilon^*$ or $\varepsilon' = \varepsilon_p$, the value of k should be obtained by the linear regression to experimental data.[43–45] Therefore, the value of k is related to materials. ε^* and ε_p can also expressed as the functions of T and $\dot{\varepsilon}$ or Z.

$$\begin{cases} \varepsilon^* = a_3 \dot{\varepsilon}^{m_3} \exp(Q_3/T) \\ \varepsilon_p = a_4 \dot{\varepsilon}^{m_4} \exp(Q_4/T) \end{cases} \qquad (6)$$

$$\begin{cases} \varepsilon^* = a_3 Z^{m_3} \\ \varepsilon_p = a_4 Z^{m_4} \end{cases} \qquad (7)$$

in which a_3, a_4, m_3, m_4, Q_3, and Q_4 are material constants. If the effect of initial grain size (d_0) on DRX kinetics behavior is considered, ε_c, ε_p, $\varepsilon_{0.5}$, and ε^* will be expressed as the function of d_0, T, and $\dot{\varepsilon}$.[7]

For a given constant T and $\dot{\varepsilon}$, the values of ε_c and ε' are constants and can be determined by Eqs. (4)–(7). Therefore, the values of X_{drx} at arbitrary strain can be directly obtained by Eq. (1). However, for inconstant T

https://doi.org/10.1557/jmr.2016.325 Published online by Cambridge University Press

and $\dot{\varepsilon}$, the values of ε_c and ε' cannot be obtained by Eqs. (4)–(7) because the value of Zener–Hollomon parameter is time-varying. Thus, the values of X_{drx} at arbitrary strain cannot be evaluated by classic DRX kinetics models. So, the classic DRX kinetics models need to be improved.

B. An improved DRX kinetics model

For predicting the DRX volume fraction under inconstant T and $\dot{\varepsilon}$, it is natural to obtain the derivative of DRX volume fraction with respect to strain $\nu_{drx}(\varepsilon)$ firstly. That is,

$$\nu_{drx}(\varepsilon) = \frac{dX_{drx}}{d\varepsilon} = \frac{\partial X_{drx}}{\partial \varepsilon} + \frac{\partial X_{drx}}{\partial T}\frac{dT(\varepsilon)}{d\varepsilon} + \frac{\partial X_{drx}}{\partial \dot{\varepsilon}}\frac{d\dot{\varepsilon}(\varepsilon)}{d\varepsilon} \tag{8}$$

in which $T(\varepsilon)$ is the temperature function of strain, and $\dot{\varepsilon}(\varepsilon)$ is the strain rate function of strain.

Then, the value of X_{drx} can be obtained by:

$$X_{drx} = \int_0^{\varepsilon} \frac{dX_{drx}}{d\varepsilon} d\varepsilon = \int_0^{\varepsilon} \nu_{drx}(\varepsilon)\, d\varepsilon \quad . \tag{9}$$

However, $T(\varepsilon)$ and $\dot{\varepsilon}(\varepsilon)$ are likely nondifferential for the practical hot deformation. That is, $dT(\varepsilon)/d\varepsilon$ and $d\dot{\varepsilon}(\varepsilon)/d\varepsilon$ often do not exist. It is hard to obtain the explicit expression of $\nu_{drx}(\varepsilon)$ or the value of $\nu_{drx}(\varepsilon)$ at a given strain. Therefore, it is almost impossible to obtain the value of X_{drx} by Eqs. (8) and (9) in the practical hot deformation.

In the study, an improved DRX kinetics model is proposed based on the hypothesis that the value of $\nu_{drx}(\varepsilon)$ only depends on the current T, $\dot{\varepsilon}$ and X_{drx}. Namely, the effects of $dT(\varepsilon)/d\varepsilon$ and $d\dot{\varepsilon}(\varepsilon)/d\varepsilon$ on DRX are neglected. The hypothesis can be explained by an example shown in Fig. 1. The material is assumed to be deformed with two stages, as shown in Fig. 1(a). In stage I, T and $\dot{\varepsilon}$ remain constant (980 °C and 0.1 s^{-1}). Therefore, the variation of X_{drx} with ε can be evaluated by classical DRX kinetics models, as shown Fig. 1(b). In stage I, the value of $\nu_{drx}(\varepsilon)$ can be evaluated by Eq. (10) because $dT(\varepsilon)/d\varepsilon$ and $d\dot{\varepsilon}(\varepsilon)/d\varepsilon$ are equal to zero:

$$\begin{cases} \nu_{drx}(\varepsilon) = \frac{dX_{drx}}{d\varepsilon} = \frac{\partial X_{drx}}{\partial \varepsilon} = \frac{nk}{\varepsilon'}(1 - X_{drx})\left[-\frac{1}{k}\ln(1 - X_{drx})\right]^{\frac{n-1}{n}} \\ \varepsilon' = f\left(T = 980\,^{\circ}\mathrm{C}, \dot{\varepsilon} = 0.01\ s^{-1}\right) \end{cases} \quad \text{when } X_{drx} > 0 \tag{10}$$

in which X_{drx} at given ε can be evaluated by classical DRX kinetics models, such as Eq. (2). ε' can be determined by the current T (980 °C) and $\dot{\varepsilon}$ (0.1 s^{-1}). The change of ν_{drx} with X_{drx} in stage I is shown in Fig. 1(c). At the end of stage I (just before the change of strain rate, Point A), $\nu_{drx,A}$ (the value of ν_{drx} at point A) can be evaluated by:

$$\begin{cases} \nu_{drx,A} = \frac{nk}{\varepsilon'}\left(1 - X_{drx,0}\right)\left[-\frac{1}{k}\ln\left(1 - X_{drx,0}\right)\right]^{\frac{n-1}{n}} \\ \varepsilon' = f\left(T = 980\,^{\circ}\mathrm{C}, \dot{\varepsilon} = 0.01\ s^{-1}\right) \end{cases} \tag{11}$$

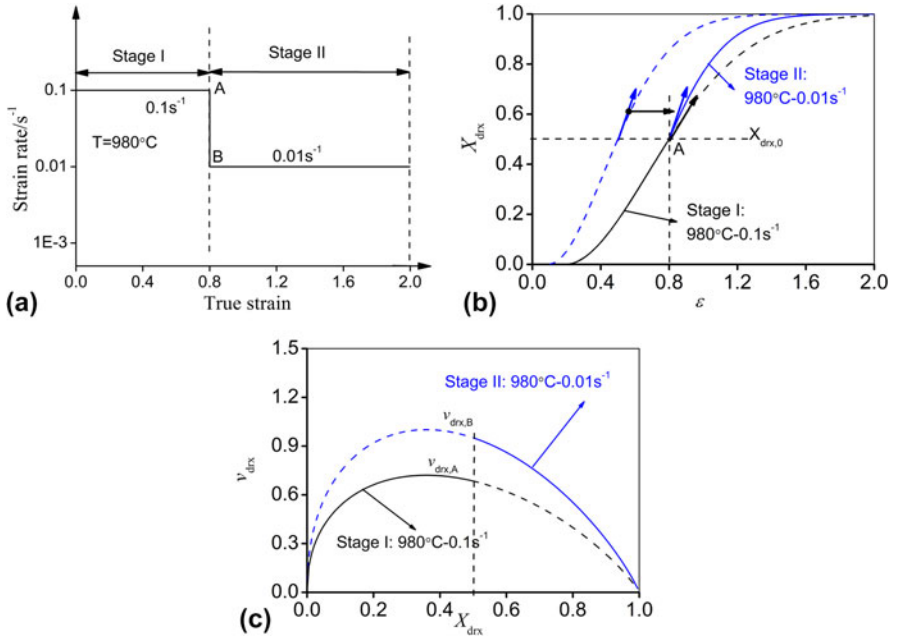


FIG. 1. Schematic diagrams of the hypothesis that the value of $\nu_{drx}(\varepsilon)$ only depends on the current T, $\dot{\varepsilon}$ and X_{drx}: (a) variation of $\dot{\varepsilon}$ with ε; (b) variation of X_{drx} with ε; (c) variation of ν_{drx} with X_{drx}.

https://doi.org/10.1557/jmr.2016.325 Published online by Cambridge University Press

in which $X_{drx,0}$ is the value of X_{drx} at the end of stage I. When the strain rate is abruptly decreased to 0.001 s^{-1} at the start of stage II [Point B, as show in Fig. 1(a)], the value of ν_{drx} will be also abruptly changed. If the effects of $dT(\varepsilon)/d\varepsilon$ and $d\dot{\varepsilon}(\varepsilon)/d\varepsilon$ on DRX are neglected, the value of ν_{drx} at the start of stage II ($\nu_{drx,B}$) can be evaluated by:

$$\begin{cases} \nu_{drx,B} = \frac{nk}{\varepsilon'}\left(1 - X_{drx,0}\right)\left[-\frac{1}{k}\ln\left(1 - X_{drx,0}\right)\right]^{\frac{n-1}{n}} \\ \varepsilon' = f\left(T = 980\,^{\circ}\mathrm{C},\ \dot{\varepsilon} = 0.001\ \mathrm{s}^{-1}\right) \end{cases}, \tag{12}$$

where $X_{drx,0}$ is also the value of X_{drx} at the start of stage II.

Therefore, an improved DRX kinetics model can be proposed according to the above hypothesis:

$$\nu_{drx}(T, \dot{\varepsilon}, X_{drx}) = \frac{nk}{\varepsilon'}(1 - X_{drx})\left[-\frac{1}{k}\ln(1 - X_{drx})\right]^{\frac{n-1}{n}} \quad \text{when } X_{drx} > 0 \quad , \tag{13}$$

where ε' is determined by the current T and $\dot{\varepsilon}$, and can be evaluated by Eqs. (4)–(7).

If $\varepsilon' = \varepsilon_{0.5} - \varepsilon_c$, Eq. (13) can be changed as:

$$\begin{cases} \nu_{drx}(T, \dot{\varepsilon}, X_{drx}) = \frac{nk}{\varepsilon_{0.5} - \varepsilon_c}(1 - X_{drx})\left[-\frac{1}{k}\ln(1 - X_{drx})\right]^{\frac{n-1}{n}} \\ \varepsilon_c = a_1 \dot{\varepsilon}^{m_1} \exp[Q_1/T] \\ \varepsilon_{0.5} = a_2 \dot{\varepsilon}^{m_2} \exp[Q_2/T] \end{cases} \quad \text{when } X_{drx} > 0 \tag{14}$$

in which k is 0.693.

Under inconstant T and $\dot{\varepsilon}$, the value of X_{drx} can be evaluated by numerical integration methods, such as rectangle rule.

$$X_{drx,l} = \sum_{i=1}^{l-1}\left(\frac{dX_{drx}}{d\varepsilon}\right)_i(\varepsilon_i - \varepsilon_{i-1}) = \sum_{i=1}^{l-1}\nu_{drx,i}(\varepsilon_i - \varepsilon_{i-1}) \tag{15}$$

in which $X_{drx,l}$ is the value of X_{drx} at the strain of ε_l, $\nu_{drx,i}$ is the value of $dX_{drx}/d\varepsilon$ at the strain ε_i. If $\Delta\varepsilon$ ($= \varepsilon_i - \varepsilon_{i-1}$) is enough small, the value of $X_{drx,l}$ obtained by Eq. (15) will be very close to the true one.

III. EXPERIMENTAL VERIFICATION OF THE IMPROVED DRX KINETICS MODEL

To verify the above improved DRX kinetics model, hot compressive tests with the inconstant strain rate were firstly done on a solution-treated Ni-based superalloy. Secondly, the DRX volume fractions of deformed specimens were obtained by analyzing optical micrographs. Finally, the comparisons between the experimental DRX volume fractions and those predicted by the improved DRX kinetics model were carried out.

A. Materials and experiments

The experimental material is a typical Ni-based superalloy with the composition (wt%) of 52.82Ni–18.96Cr–5.23Nb–3.01Mo–1.00Ti–0.59Al–0.01Co–0.03C–(bal.) Fe. Cylindrical specimens of $\phi 10\,\mathrm{mm} \times 12\,\mathrm{mm}$ were machined from a forged billet. Before hot compressive tests, all specimens were solution-treated at 1040 °C for 45 min in heat treatment furnace, then quenched by water. Figure 2 shows the starting optical microstructure of the solution-treated superalloy. The average grain size of material is about 75 μm.[34]

The experimental scheme of hot compressive tests is shown in Fig. 3. The compressive process includes two stages: I and II. The specimens were firstly compressed at the strain rate of 0.1 s^{-1} to the true strain of 0.35

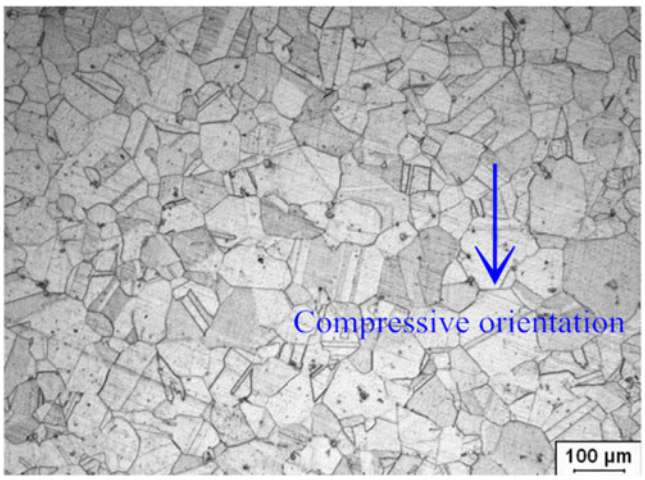


FIG. 2. The starting optical microstructure of the solution-treated superalloy.

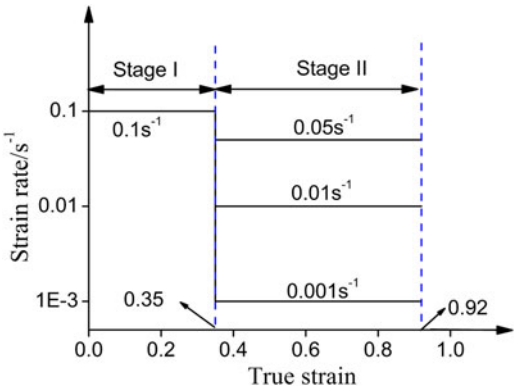


FIG. 3. Two stages of hot compressive tests.

https://doi.org/10.1557/jmr.2016.325 Published online by Cambridge University Press

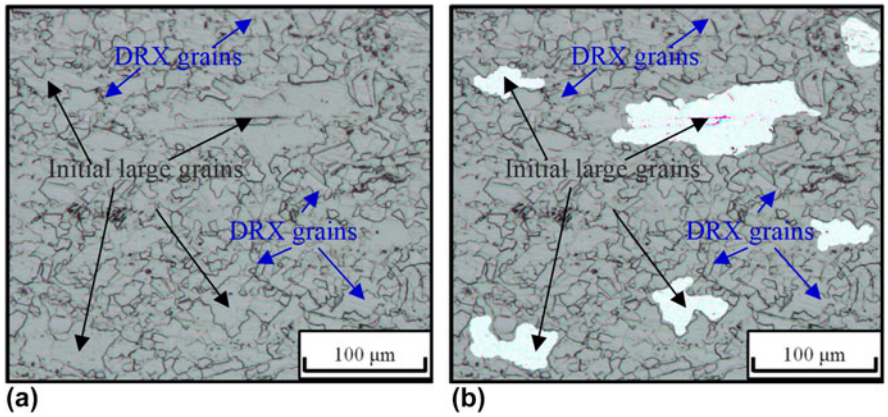


FIG. 4. Sketch maps for evaluating X_{drx} using the photoshop software: (a) the initial optical micrograph; (b) the optical micrograph which is dealt with in the Photoshop software.

(height reduction is 30%). Then, the strain rate was immediately dropped to low values (0.001, 0.01, or 0.05 s^{-1}), and the specimens continued to be compressed to the true strain of 0.92 (total height reduction is 60%). For the convenience of elaboration, the above three different inconstant strain rate cases are represented by "0.1–0.001 s^{-1}", "0.1–0.01 s^{-1}", and "0.1–0.05 s^{-1}", respectively. Three different deformation temperatures (980, 1010, and 1040 °C) were used in hot compressive tests. The hot compressive experiments were carried out on a Gleeble-3500 thermo–mechanical simulator (Dynamic Systems, Inc., Poestenkill, New York). Before the hot compression, each specimen was heated to the deformation temperature at a heating rate of 10 °C/s, and then soaked for 5 min. To minimize the friction between the specimen and dies, the tantalum foils with thickness of 0.1 mm were used during hot compression. After the compression, all specimens were immediately quenched by water. The time between unloading and quenching is about 2 s.

To observe microstructures, metallography experiments were done. The deformed specimens were firstly cut along the compressive axis section, then were mechanically polished. The polished axis section were etched in the solution of HCI (100 mL) + CH_3CH_2OH (100 mL) + $CuCl_2$ (5 g) at room temperature for 3–5 min. A Leica optical microscope (OM) was used to observe the deformed microstructures.

B. Method to evaluate the DRX volume fraction

For the experimental material, it was found that the conventional method to calculate the DRX volume fraction based on true stress–strain curves is not suitable by the authors' previous works.[34] So, the DRX volume fractions of deformed specimens were evaluated based on optical micrographs. Figure 4(a) shows the typical optical micrograph including fine DRX grains and initial large grains. Generally, the DRX volume fraction can be defined by:

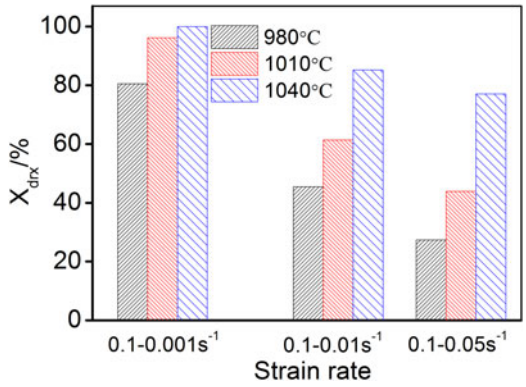


FIG. 5. DRX volume fractions in the central part of deformed specimens under tested conditions.

$$X_{drx} = \frac{A_{drx}}{A_t} = 1 - \frac{A_{initial}}{A_t} \quad (16)$$

in which A_{drx} is the area of DRX grains. A_t is the total area of optical micrograph, which is the sum of A_{drx} and $A_{initial}$. $A_{initial}$ is the area of initial grains which are not replaced by DRX grains. However, because the values of A_{drx} and $A_{initial}$ are hard to directly measure via optical micrograph, the following equation is used to evaluate X_{drx}[34]:

$$X_{drx} = 1 - \frac{N_{initial}}{N_{total}} \quad (17)$$

in which $N_{initial}$ is the number of pixel of initial grains which are not replaced by DRX grains, and N_{total} is the total number of pixel of optical micrograph. As shown in Fig. 4(b), the area of initial grains, which are not replaced by DRX grains (the white area), is chosen. The values of $N_{initial}$ and N_{total} can be directly obtained by the Photoshop software. Therefore, for a given optical micrograph, the value of X_{drx} can be evaluated by Eq. (17).

https://doi.org/10.1557/jmr.2016.325 Published online by Cambridge University Press

Three different optical micrographs in the central area were applied to obtain X_{drx} in the central part of deformed specimens ($X_{drx,c}$).

Based on the above-mentioned method, the values of X_{drx} in the central part of deformed specimens ($X_{drx,c}$) under tested conditions were obtained, as shown in Fig. 5. As shown in Fig. 5, the histories of strain rate significantly affect the DRX behavior of experimental material. The DRX volume fraction of deformed specimens increases with the decrease of strain rate in stage II. The law is similar to that under constant strain rate conditions.[34] It mainly attributes that the critical dislocation density for the nucleation of DRX grains decreases with the decrease of strain rate, and the time for the growth of small DRX grains increases. In additional, the effects of deformation temperature on DRX behaviors under inconstant strain rate conditions are also similar to those under constant strain rate conditions.[34] The DRX volume fraction of deformed specimens obviously increases with the increase of deformation temperature. It attributes to the increased mobility of grain boundaries with the increased deformation temperature.

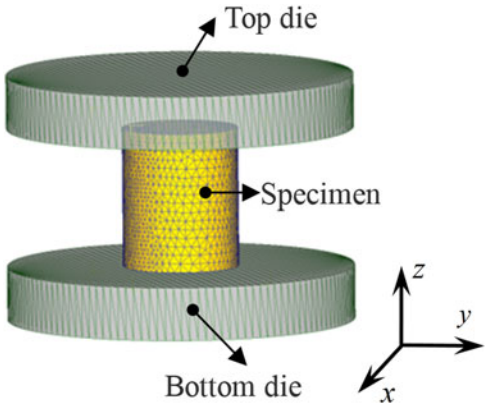


FIG. 6. Finite element model for the simulation of hot compressive process.

C. Evaluation of DRX volume fractions based on the improved DRX kinetics model

In this section, the DRX volume fractions in the central part of deformed specimens ($X_{drx,c}$) are evaluated by the improved DRX kinetics model. To consider

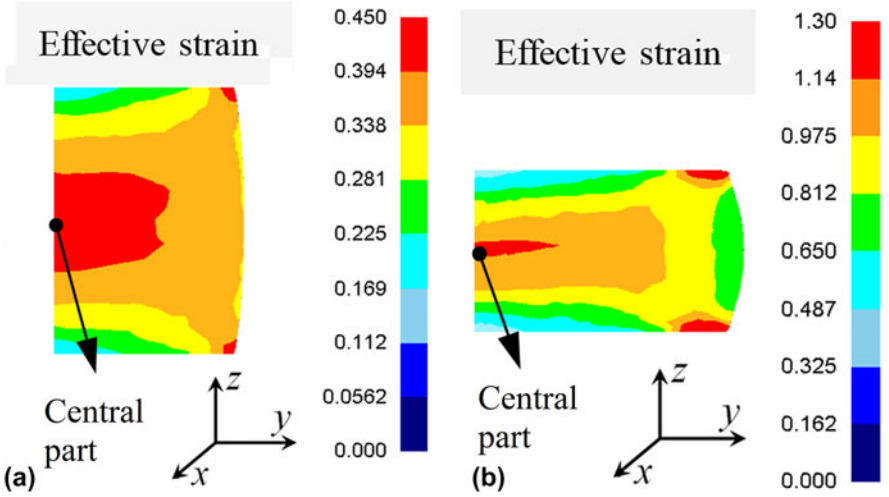


FIG. 7. Typical distributions of effective strain in the compressive axis section of deformed specimens at: (a) the end of stage I; (b) the end of stage II (half of the specimen).

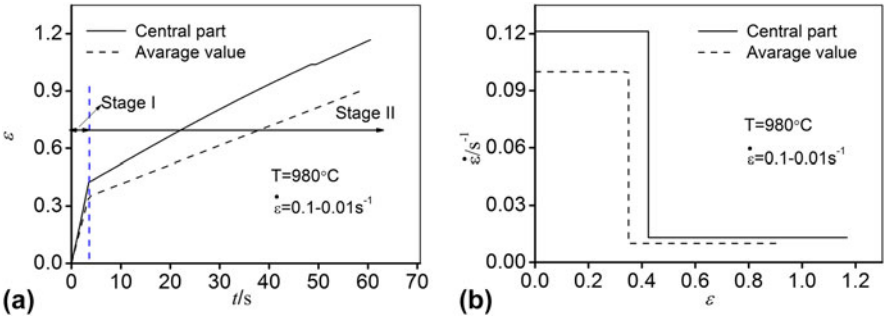


FIG. 8. Effective strains and effective strain rate in the central part of typical deformed specimen obtained by FE simulation: (a) relationship between the effective strain and time; (b) relationship between the effective strain rate and effective strain.

https://doi.org/10.1557/jmr.2016.325 Published online by Cambridge University Press

the friction-induced inhomogeneous deformation of specimens, finite element simulations have been done to obtain the strains and strain rates in the center of deformed specimens.

1. Finite element model to obtain the effective strain and strain rate

The established finite element (FE) model by DEFORM-3D software is shown in Fig. 6. The tetrahedral element was used in meshed specimen, and the number of elements is 20,000. During the simulation, a new FEM mesh on the specimen will be automatically generated whenever necessary, for example, the old mesh becomes unusable (negative Jacobian). The tabular data format is used to define the flow stress of experimental material, which is obtained from hot compressive tests.[34] The boundary conditions of FE models are the same as those of hot compressive tests.

Figure 7 shows the typical distributions of effective strain in the compressive axis section of deformed specimens. As shown in Fig. 7, it can be found that the effective strain in the central part is obviously larger than the average value. Figure 8(a) illustrates that the relationship between the effective strain and time in the central part of typical deformed specimen (the deformation temperature is 980 °C and the strain rate is "0.1–0.01 s^{-1}"). It can be found that the effective strain in the central part nearly linearly increases with time in stages I or II. Thus, the effective strain rates in stages I or II can be considered to be constant, as shown in Fig. 8(b). The values of effective strain and effective strain rate in the central part of deformed specimens obtained from FE simulation are shown in Table I.

TABLE I. The values of $\varepsilon_{I,c}$, $\varepsilon_{II,c}$, $\dot{\varepsilon}_{I,c}$, and $\dot{\varepsilon}_{II,c}$ obtained by FE simulations ($\varepsilon_{I,c}$ and $\varepsilon_{II,c}$ are the effective strains in the central part of deformed specimens at the end of stages I and II, respectively; $\dot{\varepsilon}_{I,c}$ and $\dot{\varepsilon}_{II,c}$ are the effective strain rates in the central part of deformed specimens in stages I and II, respectively).

Tested conditions					
T/°C	$\dot{\varepsilon}/s^{-1}$	$\varepsilon_{I,c}$	$\varepsilon_{II,c}$	$\dot{\varepsilon}_{I,c}/s^{-1}$	$\dot{\varepsilon}_{II,c}/s^{-1}$
980	0.1–0.001	0.424	1.20	0.121	0.00116
980	0.1–0.01	0.424	1.17	0.121	0.0111
980	0.1–0.05	0.424	1.12	0.121	0.0519
1010	0.1–0.001	0.467	1.26	0.133	0.00118
1010	0.1–0.01	0.467	1.18	0.133	0.0106
1010	0.1–0.05	0.467	1.22	0.133	0.0562
1040	0.1–0.001	0.434	1.22	0.124	0.00117
1040	0.1–0.01	0.434	1.16	0.124	0.0108
1040	0.1–0.05	0.434	1.18	0.124	0.0557

2. Evaluation of DRX volume fractions in the central part of deformed specimens

The classic DRX kinetics models for the experimental material (a typical solution-treated Ni-based superalloy) were reported in authors' previous work.[34]

$$\begin{cases} X_{\mathrm{drx}} = 1 - \exp\left[-0.693\left(\frac{\varepsilon-\varepsilon_c}{\varepsilon_{0.5}-\varepsilon_c}\right)^{1.8}\right] \\ \varepsilon_{0.5} = 6.43937\times10^{-6}\,\dot{\varepsilon}^{0.14281982}\exp(16038.638/T) \\ \varepsilon_c = 0.2315\varepsilon_{0.5} \end{cases} \tag{18}$$

in which X_{drx} is the DRX volume fraction, ε is the strain, ε_c is the critical strain for the onset of DRX, $\varepsilon_{0.5}$ is the strain for 50% DRX, T is the deformation temperature (unit: K), and $\dot{\varepsilon}$ is the strain rate (unit: s^{-1}).

Substituting the material constants of Eq. (18) into Eq. (14), the improved DRX kinetics model for predicting

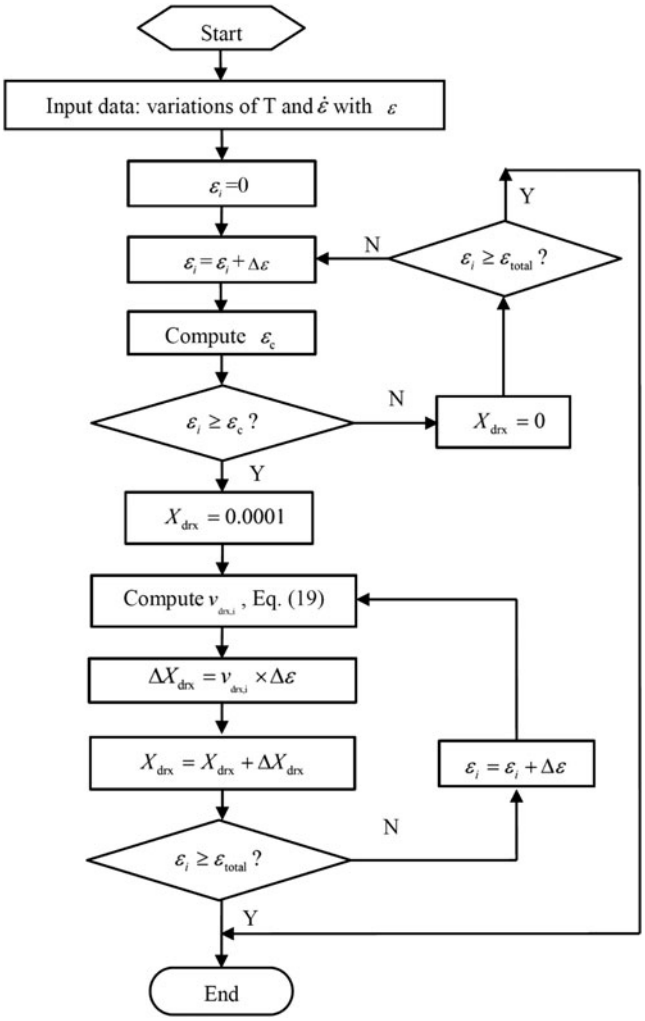


FIG. 9. Flow chart to evaluate the DRX volume fractions based on the improved DRX kinetics model.

https://doi.org/10.1557/jmr.2016.325 Published online by Cambridge University Press

DRX behavior under inconstant deformation temperature and strain rate conditions can be obtained as:

$$\begin{cases} \nu_{\mathrm{drx}}(T,\dot{\varepsilon},X_{\mathrm{drx}}) = \frac{1.2474}{\varepsilon_{0.5}-\varepsilon_{\mathrm{c}}}(1-X_{\mathrm{drx}})\left[-\frac{1}{0.693}\ln(1-X_{\mathrm{drx}})\right]^{\frac{4}{9}} \\ \varepsilon_{\mathrm{c}} = 1.49\times10^{-6}\,\dot{\varepsilon}^{0.14281982}\,\exp(16038.638/T) \\ \varepsilon_{0.5} = 6.43937\times10^{-6}\,\dot{\varepsilon}^{0.14281982}\,\exp(16038.638/T) \\ \qquad\qquad \text{when } X_{\mathrm{drx}} > 0 \end{cases} \tag{19}$$

In order to evaluate the DRX volume fractions, a computer program based on the improved DRX kinetics model is developed. The flow chart is shown in Fig. 9. In Fig. 9, $\varepsilon_{\mathrm{total}}$ is the total effective strain, which is equal to $\varepsilon_{\mathrm{II,c}}$ for the central part of deformed specimens. $\Delta\varepsilon$ is the strain increment which should be enough small. In this paper, it is enough that $\Delta\varepsilon$ is 0.001 to accurately predict DRX volume fractions. Based on the data shown in Table I, the DRX volume fractions in the central part of deformed specimens under tested conditions are obtained, as listed in Table II.

TABLE II. Experimental and predicted $X_{\mathrm{drx,c}}$.

Deformation conditions		Experimental	Predicted	Absolute
T/°C	$\dot{\varepsilon}/\mathrm{s}^{-1}$	$X_{\mathrm{drx,c}}$/%	$X_{\mathrm{drx,c}}$/%	error/%
980	0.1–0.001	80.52	59.16	21.36
980	0.1–0.01	45.50	37.72	7.78
980	0.1–0.05	27.38	24.92	2.46
1010	0.1–0.001	96.16	84.59	11.57
1010	0.1–0.01	61.38	61.77	−0.39
1010	0.1–0.05	43.93	51.72	−7.79
1040	0.1–0.001	100.00	96.08	3.92
1040	0.1–0.01	85.20	82.76	2.44
1040	0.1–0.05	77.08	72.74	4.34

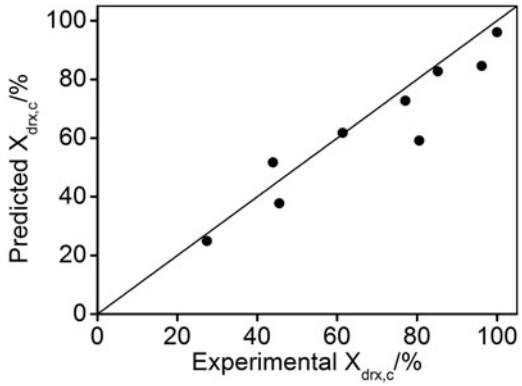


FIG. 10. Comparisons between the experimental and predicted $X_{\mathrm{drx,c}}$.

D. Comparisons between the experimental and predicted DRX volume fractions

The comparisons between the experimental and predicted $X_{\mathrm{drx,c}}$ are done, as shown in Fig. 10. It shows that the predicted $X_{\mathrm{drx,c}}$ well agree with the experimental ones. The absolute errors between the experimental and predicted $X_{\mathrm{drx,c}}$ are evaluated, as listed in Table II. The absolute errors are smaller than 8% for most cases. It indicates that the improved DRX kinetics model can well predict the DRX behavior of the solution-treated Ni-based superalloy under inconstant deformation temperature and strain rate conditions.

IV. CONCLUSIONS

In practical industrial production, the deformation temperature and strain rate of forgings are often time-varying. However, the classical DRX kinetics models can only describe the DRX behavior under constant deformation temperature and strain rate conditions. Therefore, an improved DRX kinetics model, which can describe the DRX behavior under inconstant deformation conditions, is proposed. To verify the improved DRX kinetics model, the hot compressive tests with abruptly-changed strain rate were done on a solution-treated Ni-based superalloy. The comparisons between the experimental and predicted DRX volume fractions indicate that the improved DRX kinetics model is suitable for describing the DRX behavior of metals or alloys under inconstant deformation conditions.

ACKNOWLEDGMENTS

This work was supported by National Natural Science Foundation of China (Nos. 51305466, 51375502), National Key Basic Research Program (Grant No. 2013CB035801), State key laboratory of High Performance Complex Manufacturing (No. zzyjkt2014-01), the Project of Innovation-driven Plan in Central South University (Grant No. 2016CX008), the Natural Science Foundation for Distinguished Young Scholars of Hunan Province (Grant No. 2016JJ1017), and Program of Chang Jiang Scholars of Ministry of Education (Grant No. Q2015140), China.

REFERENCES

1. H.J. McQueen: Development of dynamic recrystallization theory. *Mater. Sci. Eng., A* **387–389**, 203 (2004).
2. J. De Jaeger, D. Solas, O. Fandeur, J. Schmitt, and C. Rey: 3D numerical modeling of dynamic recrystallization under hot working: Application to Inconel 718. *Mater. Sci. Eng., A* **33**, 646 (2015).
3. H. Beladi and P.D. Hodgson: Effect of carbon content on the recrystallization kinetics of Nb-steels. *Scr. Mater.* **56**, 1059 (2007).
4. S. Vervynckt, K. Verbeken, P. Thibaux, and Y. Houbaert: Recrystallization–precipitation interaction during austenite hot deformation of a Nb microalloyed steel. *Mater. Sci. Eng., A* **528**, 5519 (2011).
5. G.L. Ji, F.G. Li, Q.H. Li, H.Q. Li, and Z. Li: Research on the dynamic recrystallization kinetics of Aermet100 steel. *Mater. Sci. Eng., A* **527**, 2350 (2010).

https://doi.org/10.1557/jmr.2016.325 Published online by Cambridge University Press

6. S.D. Gu, L.W. Zhang, C. Zhang, J.H. Ruan, and Y. Zhen: Modeling the effects of processing parameters on dynamic recrystallization behavior of deformed 38MnVS6 steel. *J. Mater. Eng. Perform.* **24**, 1790 (2015).
7. M.S. Chen, Y.C. Lin, and X.S. Ma: The kinetics of dynamic recrystallization of 42CrMo steel. *Mater. Sci. Eng., A* **556**, 260 (2012).
8. B.C. Zhao, T. Zhao, G.Y. Li, and Q. Lu: The kinetics of dynamic recrystallization of a low carbon vanadium-nitride microalloyed steel. *Mater. Sci. Eng., A* **604**, 117 (2014).
9. D. Xu, M.Y. Zhu, Z.Y. Tang, and C. Sun: Determination of the dynamic recrystallization kinetics model for SCM435 steel. *J. Wuhan. Univ. Technol., Mater. Sci. Ed.* **28**, 819 (2013).
10. Y.G. Liu, M.Q. Li, and J. Luo: The modelling of dynamic recrystallization in the isothermal compression of 300M steel. *Mater. Sci. Eng., A* **574**, 1 (2013).
11. H. Mirzadeh and A. Najafizadeh: Prediction of the critical conditions for initiation of dynamic recrystallization. *Mater. Des.* **31**, 1174 (2010).
12. Y.W. Xu, D. Tang, Y. Song, and X.G. Pan: Dynamic recrystallization kinetics model of X70 pipeline steel. *Mater. Des.* **39**, 168 (2012).
13. S. Mandal, P.V. Sivaprasad, and R.K. Dube: Modeling microstructural evolution during dynamic recrystallization of Alloy D9 using artificial neural network. *J. Mater. Eng. Perform.* **16**, 672 (2007).
14. A. Momeni and K. Dehghani: Prediction of dynamic recrystallization kinetics and grain size for 410 martensitic stainless steel during hot deformation. *Met. Mater. Int.* **16**, 843 (2010).
15. G.R. Ebrahimi, H. Keshmiri, A. Momeni, and M. Mazinani: Dynamic recrystallization behavior of a superaustenitic stainless steel containing 16%Cr and 25%Ni. *Mater. Sci. Eng., A* **528**, 7488 (2011).
16. G.R. Stewart, J.J. Jonas, and F. Montheillet: Kinetics and critical conditions for the initiation of dynamic recrystallization in 304 stainless steel. *ISIJ Int.* **44**, 1581 (2004).
17. A. Marchattiwar, A. Sarkar, J.K. Chakravartty, and B.P. Kashyap: Dynamic recrystallization during hot deformation of 304 austenitic stainless steel. *J. Mater. Eng. Perform.* **22**, 2168 (2013).
18. D. Ohadi, M.H. Parsa, and H. Mirzadeh: Development of dynamic recrystallization maps based on the initial grain size. *Mater. Sci. Eng., A* **565**, 90 (2013).
19. G.R. Ebrahimi, H. Keshmiri, A.R. Maldad, and A. Momeni: Dynamic recrystallization behavior of 13%Cr martensitic stainless steel under hot working condition. *J. Mater. Sci. Technol.* **28**, 467 (2012).
20. M. El Wahabi, L. Gavard, F. Montheillet, J.M. Cabrera, and J.M. Prado: Effect of initial grain size on dynamic recrystallization in high purity austenitic stainless steels. *Acta Mater.* **53**, 4605 (2005).
21. G.L. Ji, Q. Li, and L. Li: The kinetics of dynamic recrystallization of Cu–0.4Mg alloy. *Mater. Sci. Eng., A* **586**, 197 (2013).
22. P. Changizian, A. Zarei-Hanzaki, and H.R. Abedi: On the recrystallization behavior of homogenized AZ81 magnesium alloy: The effect of mechanical twins and γ precipitates. *Mater. Sci. Eng., A* **558**, 44 (2012).
23. D.X. Zhang, X.Y. Yang, H. Sun, Y. Li, J. Wang, Z.R. Zhang, Y.X. Ye, and T. Sakai: Dynamic recrystallization behaviors and the resultant mechanical properties of a Mg–Y–Nd–Zr alloy during hot compression after aging. *Mater. Sci. Eng., A* **640**, 51 (2015).
24. T.C. Xu, X.D. Peng, J. Qin, Y.F. Chen, Y. Yang, and G.B. Wei: Dynamic recrystallization behavior of Mg–Li–Al–Nd duplex alloy during hot compression. *J. Alloys Compd.* **639**, 79 (2015).
25. H.C. Xiao, S.N. Jiang, B. Tang, W.H. Hao, Y.H. Gao, Z.Y. Chen, and C.M. Liu: Hot deformation and dynamic recrystallization behaviors of Mg–Gd–Y–Zr alloy. *Mater. Sci. Eng., A* **628**, 311 (2015).
26. B.J. Lv, J. Peng, D.W. Shi, A.T. Tang, and F.S. Pan: Constitutive modeling of dynamic recrystallization kinetics and processing maps of Mg–2.0Zn–0.3Zr alloy based on true stress–strain curves. *Mater. Sci. Eng., A* **560**, 727 (2013).
27. N. Cui, F.T. Kong, X.P. Wang, Y.Y. Chen, and H.T. Zhou: Hot deformation behavior and dynamic recrystallization of a β-solidifying TiAl alloy. *Mater. Sci. Eng., A* **652**, 231 (2016).
28. K. Tan, J. Li, Z.J. Guan, J.B. Yang, and J.X. Shu: The identification of dynamic recrystallization and constitutive modeling during hot deformation of Ti55511 titanium alloy. *Mater. Des.* **84**, 204 (2015).
29. Y.Q. Ning, Z.K. Yao, M.W. Fu, and H.Z. Guo: Recrystallization of the hot isostatic pressed nickel-base superalloy FGH4096: I. Microstructure and mechanism. *Mater. Sci. Eng., A* **528**, 8065 (2011).
30. H.B. Zhang, K.F. Zhang, H.P. Zhou, Z. Lu, C.H. Zhao, and X.L. Yang: Effect of strain rate on microstructure evolution of a nickel-based superalloy during hot deformation. *Mater. Des.* **80**, 51 (2015).
31. X.M. Chen, Y.C. Lin, D.X. Wen, J.L. Zhang, and M. He: Dynamic recrystallization behavior of a typical nickel-based superalloy during hot deformation. *Mater. Des.* **57**, 568 (2014).
32. Y.C. Lin, X.Y. Wu, X.M. Chen, J. Chen, D.X. Wen, J.L. Zhang, and L.T. Li: EBSD study of a hot deformed nickel-based superalloy. *J. Alloys Compd.* **640**, 101 (2015).
33. Y.C. Lin, D.G. He, M.S. Chen, X.M. Chen, C.Y. Zhao, X. Ma, and Z.L. Long: EBSD analysis of evolution of dynamic recrystallization grains and δ phase in a nickel-based superalloy during hot compressive deformation. *Mater. Des.* **97**, 13 (2016).
34. M.S. Chen, Y.C. Lin, K.K. Li, and Y. Zhou: A new method to establish dynamic recrystallization kinetics model of a typical solution-treated Ni-based superalloy. *Comput. Mater. Sci.* **122**, 150 (2016).
35. H. Riedel and J. Svoboda: A model for strain hardening, recovery, recrystallization and grain growth with applications to forming processes of nickel base alloys. *Mater. Sci. Eng., A* **665**, 175 (2016).
36. H.Y. Wu, L.X. Du, and X.H. Liu: Dynamic recrystallization and precipitation behavior of Mn–Cu–V weathering steel. *J. Mater. Sci. Technol.* **27**, 1131 (2011).
37. H. Hallberg, B. Svendsen, T. Kayser, and M. Ristinmaa: Microstructure evolution during dynamic discontinuous recrystallization in particle-containing Cu. *Comput. Mater. Sci.* **84**, 327 (2014).
38. I. Mejía, A. Bedolla-Jacuinde, C. Maldonado, and J.M. Cabrera: Determination of the critical conditions for the initiation of dynamic recrystallization in boron microalloyed steels. *Mater. Sci. Eng., A* **528**, 4133 (2011).
39. G.Z. Quan, S.A. Pu, H.R. Wen, Z.Y. Zou, and J. Zhou: Quantitative analysis of dynamic softening behaviors induced by dynamic recrystallization for Ti–10V–2Fe–2Al alloy. *High Temp. Mater. Process.* **34**, 549 (2015).
40. J.J. Jonas, X. Quelennec, L. Jiang, and É. Martin: The Avrami kinetics of dynamic recrystallization. *Acta Mater.* **57**, 2748 (2009).
41. J. Liu, Z. Cui, and L. Ruan: A new kinetics model of dynamic recrystallization for magnesium alloy AZ31B. *Mater. Sci. Eng., A* **529**, 300 (2011).
42. H. Won Lee and Y.T. Im: Numerical modeling of dynamic recrystallization during nonisothermal hot compression by cellular automata and finite element analysis. *Int. J. Mech. Sci.* **52**, 1277 (2010).
43. Y. Xu, L.X. Hu, and Y. Sun: Deformation behaviour and dynamic recrystallization of AZ61 magnesium alloy. *J. Alloys Compd.* **580**, 262 (2013).

https://doi.org/10.1557/jmr.2016.325 Published online by Cambridge University Press

44. J.B. Li, Y. Liu, Y. Wang, B. Liu, and Y.H. He: Dynamic recrystallization behavior of an as-cast TiAl alloy during hot compression. *Mater. Charact.* **97**, 169 (2014).
45. J.B. Jia, K.F. Zhang, and Z. Lu: Dynamic recrystallization kinetics of a powder metallurgy Ti–22Al–25Nb alloy during hot compression. *Mater. Sci. Eng., A* **607**, 630 (2014).
46. H.L. Wei, G.Q. Liu, X. Xiao, and M.H. Zhang: Dynamic recrystallization behavior of a medium carbon vanadium microalloyed steel. *Mater. Sci. Eng., A* **573**, 215 (2013).
47. L. Cheng, H. Chang, B. Tang, H.C. Kou, and J.S. Li: Deformation and dynamic recrystallization behavior of a high Nb containing TiAl alloy. *J. Alloys Compd.* **552**, 363 (2013).
48. D.L. OuYang, M.W. Fu, and S.Q. Lu: Study on the dynamic recrystallization behavior of Ti-alloy Ti–10V–2Fe–3V in β processing via experiment and simulation. *Mater. Sci. Eng., A* **619**, 26 (2014).
49. X.C. Li, L.L. Duan, J.W. Li, and X.C. Wu: Experimental study and numerical simulation of dynamic recrystallization behavior of a micro-alloyed plastic mold steel. *Mater. Des.* **66**, 309 (2015).

https://doi.org/10.1557/jmr.2016.325 Published online by Cambridge University Press